ELSEVIER

Genesis of monazite and Y zoning in garnet from the Black Hills, South Dakota

Panseok Yang *, David Pattison

Department of Geology and Geophysics, University of Calgary, 2500 University Drive N.W., Calgary, Alberta, Canada T2N 1N4

Abstract

The paragenesis of monazite in metapelitic rocks from the contact aureole of the Harney Peak Granite, Black Hills, South Dakota, was investigated using zoning patterns of monazite and garnet, electron microprobe dating of monazite, bulk-rock compositions, and major phase mineral equilibria. The area is characterized by low-pressure and high-temperature metamorphism with metamorphic zones ranging from garnet to sillimanite zones. Garnet porphyroblasts containing euhedral Y annuli are observed from the garnet to sillimanite zones. Although major phase mineral equilibria predict resorption of garnet at the staurolite isograd and regrowth at the andalusite isograd, textural and mass balance analyses suggest that the formation of the Y annuli is not related to the resorption-and-regrowth of garnet having formed instead during garnet growth in the garnet zone. Monazite grains in Black Hills pelites were divided into two generations on the basis of zoning patterns of Y and U: monazite 1 with low-Y and -U and monazite 2 with high-Y and -U. Monazite 1 occurs in the garnet zone and persists into the sillimanite zone as cores shielded by monazite 2 which starts to form in the andalusite zone. Pelites containing garnet porphyroblasts with Y annuli and monazite 1 with patchy Th zoning are more calcic than those with garnet with no Y annuli and monazite with concentric Th zoning. Monazite 1 is attributed to breakdown of allanite in the garnet zone, additionally giving rise to the Y annuli observed in garnet. Monazite 2 grows in the andalusite zone, probably at the expense of garnet and monazite 1 in the andalusite and sillimanite zones. The ages of the two different generations of monazite are within the precision of chemical dating of electron microprobe. The electron microprobe ages of all monazites from the Black Hills show a single ca. 1713 Ma population, close to the intrusion age of the Harney Peak Granite (1715 Ma). This study demonstrates that Y zoning in garnet and monazite are critical to the interpretation of monazite petrogenesis and therefore monazite ages.
© 2005 Elsevier B.V. All rights reserved.

Keywords: Monazite; Allanite; Garnet; Y annuli; Chemical dating of monazite; Black Hills; South Dakota

1. Introduction

The focus of metamorphic petrology is now moving from the determination of *P–T* paths to *P–T–t* paths.

P–T–t paths provide opportunities to estimate the dynamics of mountain-building processes. To construct internally consistent *P–T–t* paths, metamorphic ages and *P–T* conditions should be determined simultaneously using radioactive accessory minerals such as monazite and zircon. While metamorphic temperatures can be potentially estimated by the monazite–xenotime solvus thermometer (Gratz and Heinrich, 1997, 1998; Heinrich et al., 1997; Andrehs and Heinrich, 1998; Pyle et al., 2001), garnet–monazite thermometer (Pyle et al.,

* Corresponding author. Present address: Department of Geological Sciences, University of Manitoba, Winnipeg, Manitoba, Canada R3T 2NT.

E-mail addresses: yangp@cc.umanitoba.ca (P. Yang), pattison@ucalgary.ca (D. Pattison).

2001), and garnet–xenotime thermometer (Pyle and Spear, 2000), the estimation of metamorphic pressure is difficult because the Y and REE exchange reactions generally involve small changes in volume. In addition, the restricted stability field of xenotime to mostly garnet zone in garnet-bearing pelitic rocks reduces the applicability of the monazite–xenotime and garnet–xenotime thermometers. These problems can be overcome by combining the paragenesis of accessory phases with equilibria of major phases. The latter provide independent estimation of metamorphic pressure and temperature.

This study focuses on Y zoning in garnet and monazite to investigate the parageneses of the Y-rich accessory phases such as monazite and xenotime from greenschist to amphibolite facies metapelitic rocks in the aureole of the Harney Peak Granite, Black Hills, South Dakota. Schwandt et al. (1996) reported abrupt humps in the Y zoning profiles of garnet porphyroblasts in the staurolite zone of the Black Hills pelites, resembling discontinuous Y annuli in garnet observed in staurolite and higher grade regionally metamorphosed pelites reported elsewhere (e.g., Chernoff

and Carlson, 1999; Pyle and Spear, 1999, 2000; Yang and Rivers, 2002; Kohn and Malloy, 2004). The origin of the Y annuli in garnet has been widely attributed to garnet resorption at the staurolite isograd followed by garnet regrowth at the aluminum silicate isograd (e.g., Pyle and Spear, 1999; Kohn and Malloy, 2004). It has also been commonly interpreted that the resorption of garnet at the staurolite isograd triggered the first major growth of monazite in the prograde sequence (Smith and Barreiro, 1990; Kohn and Malloy, 2004), resulting in the interpretation that measured monazite ages correspond to the age of staurolite growth. In this study, the origins of Y annuli in pelitic garnet are investigated in terms of (1) discontinuous breakdown of Y-rich accessory minerals such as xenotime, monazite, allanite, and zircon, (2) resorption and regrowth of garnet at major-phase isograds, (3) infiltration of Y-rich metamorphic fluids, and (4) changes in garnet growth rates. Major phase reactions were modeled in fixed bulk-rock compositions, and then linked to the paragenesis of accessory phases through Y zoning in garnet and monazite and mass balance constraints.
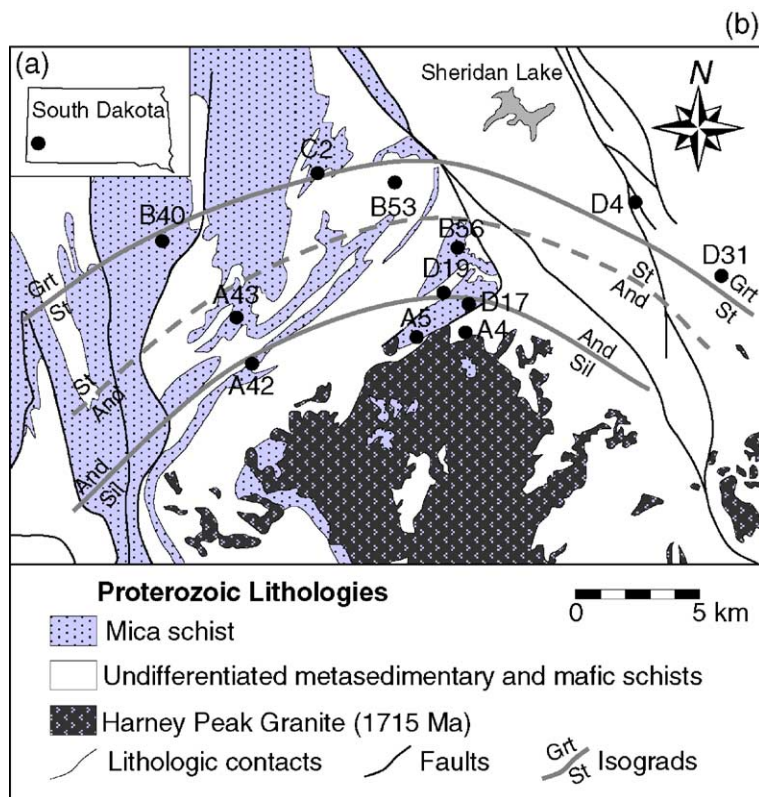
Fig. 1. Simplified geologic map of the southern Black Hills, South Dakota (modified from DeWitt et al., 1989), showing locations of investigated metapelites and metamorphic isograds. The location of the andalusite isograd is not certain. Inset shows Black Hills relative to South Dakota. Mineral abbreviations are from Kretz (1983).

2. Geologic setting

The Precambrian core of the Black Hills uplift is located in southwestern South Dakota (Fig. 1a). The core consists of a thick stratigraphic sequence of Proterozoic metasedimentary and metavolcanic phyllites and schists intruded by the Harney Peak Granite (HPG, Fig. 1b). A minimum of three periods of deformation and at least two phases of metamorphism have been identified in the area (Redden et al., 1982, 1990; DeWitt et al., 1986; Terry and Friberg, 1990; Helms and Labotka, 1991; Dahl and Frei, 1998; Dahl et al., 2005; Nabelek et al., 2005). The first deformation folded a stratigraphic sequence of turbidites and volcanic rocks into east-northeast-trending, north directed nappes and thrusts. The second deformation refolded the nappes into steep south plunging isoclinal folds trending north to northwest. The intrusion of the HPG caused domal structures and late faulting around the pluton.

Dynamothermal metamorphism associated with the uplift event is believed to have caused the anatexis of Proterozoic metasedimentary rocks, resulting in emplacement of S-type granites and low-pressure, high-temperature contact metamorphism (Duke et al., 1988; Shearer et al., 1992; Terry and Friberg, 1990;

Helms and Labotka, 1991). P–T conditions at the peak of metamorphism were estimated from mineral equilibria in pelitic schists by Helms and Labotka (1991). Temperature ranged from 469–500 °C in the garnet zone to 528–555 °C in the sillimanite zone over a pressure range of 2.0–4.4 kbar. Around the HPG, there are numerous pegmatites, some of which are enriched in trace and rare earth elements (Shearer et al., 1992).

Mineral assemblages of the pelites selected for this study are given in Table 1. Garnet, biotite, muscovite, plagioclase, and quartz are present in all samples with chlorite, staurolite, andalusite, and sillimanite as additional phases depending on metamorphic grade and bulk-rock compositions. Accessory mineral assemblages of all investigated pelites include ilmenite, rutile, tourmaline, monazite, apatite and zircon. Xenotime occurs in sample B40 as inclusions in garnet and in sample D19 as a matrix mineral. Allanite was sought but not found in metapelites above the garnet zone. In this study, metamorphic isograds were mapped in pelitic schists based on the metamorphic assemblages Grt–Bt ± Chl (garnet zone), Grt–St–Bt (staurolite zone), Grt–And–Bt (andalusite zone), and Grt–Sil–Bt (sillimanite zone) from 168 samples (Fig. 1b). The andalusite zone is not well defined in this study because of the small number of andalusite-bearing rocks. The Black Hills mineral assemblage sequence places it in facies series 2b of Pattison and Tracy (1991).

3. Analytical methods

Quantitative chemical analyses of garnet and monazite were determined by wavelength-dispersive X-ray analysis using the JEOL JXA 8200 electron microprobe at the University of Calgary. Analytical conditions include an accelerating potential of 15 keV and Faraday cup currents of 20 and 500 nA for major and trace element analysis, respectively, in garnet and an accelerating potential of 15 keV and a Faraday cup current of 50 nA for all elements in monazite analysis. Electron beams were defocused to 1 and 5 μm diameters for garnet and monazite analyses, respectively.

Element distribution maps of Mn, Ca, and Y in garnet and Th, U, and Y in monazite were collected using an accelerating voltage of 15 keV, Faraday cup currents of 1 μA for garnet and 500 nA for monazite, step sizes of 5–10 μm/pixel for garnet and 0.5–1 μm/pixel for monazite, and counting times ranging from 50 to 300 ms/pixel. Element distribution maps were

Table 1
Mineral assemblages of the Black Hills pelites

Samples	Als	St	Chl	Xen
Garnet zone				
C2			X	
D4			X	
D31			X	
Staurolite zone				
B40		X	X	I
B53	A	X		
Andalusite-zone				
A43		X		
B56		X		
D19	A	X		X
Sillimanite zone				
A4	S	X		
A5	S			
A42	A/S			
D17	S			

Grt, Bt, Ms, Pl, Mnz, Ap, Zrn, Ilm, Rt, and Tur are present in all samples. Mineral abbreviations from Kretz (1983).
X: mineral identified in sample.
I: xenotime present as inclusions in garnet.
Als: aluminum silicates, A: andalusite; S: sillimanite.

processed using the public domain program NIH Image v. 1.61b12 (Rasband, 1998).

Analytical settings for electron microprobe chemical dating of monazite are given in Table 2. Beam conditions were an accelerating voltage of 15 keV, a beam current of 150–200 nA on the Faraday cup, a beam size of 5–10 μm, and a counting time of 3 min on Pb peak. X-ray intensities of Pb and U were measured on M_β lines. Although the X-ray intensity of Pb M_β is about 80% that of the M_α line, Pb M_β is measured in this study because of the absence of interference from Th and Y. Pb was counted under Xe gas on two different PET crystals simultaneously to improve precision and accuracy. Raw intensities of U were corrected for a peak overlap from Th. Th intensity was measured on the M_α line. In addition Ce, P, Y, and La were determined for ZAF corrections while the rest of the undetermined elements were treated as Nd (Table 2).

Accessory phases were identified using back-scattered electron imaging and energy-dispersive spectroscopy. Modes of monazite for two samples (B40 and D19) were determined via digital back-scattered electron images at a 1.3 μm pixel resolution for half area of each thin section. The modes vary by 10% depending on the degree of threshold in the digital images, which was set at minimum level for the resolution of monazite from other minerals.

4. Results

4.1. Whole-rock chemistry

Whole-rock compositions of selected Black Hills pelites determined by X-ray fluorescence spectrometry at McGill University are listed in Table 3, together with the average pelite compositions of Shaw (1956), Mahar et al. (1997), and Tinkham et al. (2001). Compared to the three average pelites, Black Hills pelites are characterized by slightly higher X_{FeO} [$= FeO/(FeO+MgO+MnO)$] values, ranging from 0.58 to 0.62, but lower X_{CaO} [$= CaO/(CaO+Na_2O)$] values, ranging from 0.21 to 0.37. The majority of the Black Hills pelites show low X_{MnO} [$= MnO/(FeO+MgO+MnO)$] values, ranging from 0.005 to 0.01, with samples C2 and B40 distinctively richer in Mn ($X_{MnO} = 0.016$ and 0.018). In an AFM diagram (Fig. 2), the majority of the Black Hills pelites plot in the sub-aluminous field (i.e., project below the garnet–chlorite tie-line in the AFM projection), except for sample D19 which plots above the garnet–chlorite tie-line.

4.2. Mineral assemblage modeling

P–T mineral assemblage stability diagrams were calculated for Na_2O–CaO–MnO–K_2O–FeO–MgO–Al_2O_3–SiO_2–H_2O (NCMnKFMASH) system using

Table 2
Electron microprobe settings for monazite chemical age calibration and analysis

Element	Crystal	Detector gases	Peak	Gain (V)	Bias (V)	Base (V)	Window (V)	+Bkg (mm)	−Bkg (mm)	Time (s)
For calibration										
Th	PET	Ar	M_α	1746	8	1.55	4.55	4	4	20
La	PET	Ar	L_α	1724	8	0.5	5.65	4.2	3.8	20
Pb	PET	Xe	M_β	1730	128	2.65	3	13.4	5	20
Pb	PETH	Xe	M_β	1730	128	2.65	3	13.4	5	20
U	PET	Ar	M_β	1752	8	2.05	3.95	4	3	20
Ce	PET	Ar	L_α	1728	8	0.4	5.6	4	3	20
Y	PET	Ar	L_α	1724	8	1.7	4.1	5	4	20
P	PET	Ar	K_α	1778	8	1.8	4.5	4	3	20
For analysis										
Th	PET	Ar	M_α	1746	8	1.55	4.55	2.7	3	60
La	PET	Ar	L_α	1724	8	0.5	5.65	3.2	1.8	40
Pb	PET	Xe	M_β	1730	128	2.65	3	3	2	180
Pb	PETH	Xe	M_β	1730	128	2.65	3	3	2	180
U	PET	Ar	M_β	1752	8	2.05	3.95	2.5	3	160
Ce	PET	Ar	L_α	1728	8	0.4	5.6	1.5	1.5	20
Y	PET	Ar	L_α	1724	8	1.7	4.1	2	2.5	60
P	PET	Ar	K_α	1778	8	1.8	4.5	4	3	20

Standards: $LaPO_4$ (La), YPO_4 (Y), $CePO_4$ (Ce and P), $Pb_5(PO_4)_3Cl$ (Pb), ThO_2 (Th), and UO_2 (U).
PETH: Large PET crystal with 100 mm Rowland circle radius.
Counting time: peak counting times.

Table 3
Whole-rock compositions

Sample	S	M	T	Grt-zone C-2	D-31	St-zone A-43	B-40	B-56	And-zone B-53	D-19	Sil-zone A-4	A-5	A-42	D-17
(Wt.% oxides and ppm)														
SiO_2	61.54	59.80	60.78	60.02	68.90	66.51	58.99	64.10	60.51	58.00	76.54	73.30	62.48	62.14
TiO_2	0.82			0.70	0.68	0.59	0.78	0.73	0.68	0.74	0.54	0.58	0.66	0.72
$Al2O_3$	16.95	16.57	16.88	18.93	14.73	16.05	18.94	17.18	18.90	23.83	11.41	13.02	17.13	20.15
$FeO^{\#}$	6.02	5.81	6.87	7.02	5.98	6.70	8.55	6.78	6.88	8.09	3.65	3.96	7.94	4.47
MnO		0.10	0.13	0.19	0.07	0.08	0.24	0.11	0.10	0.07	0.05	0.06	0.07	0.05
MgO	2.52	2.62	3.44	2.73	2.35	2.31	2.85	2.42	2.45	2.67	1.20	1.43	2.78	1.59
CaO	1.76	1.09	1.21	0.26	0.24	0.79	0.30	0.52	0.40	0.26	0.71	0.87	0.36	0.79
Na_2O	1.84	1.73	1.65	1.09	0.46	1.62	0.67	1.43	1.10	0.51	2.20	1.93	1.28	1.68
K_2O	3.45	3.53	3.70	5.48	4.29	3.69	4.79	4.45	5.25	3.96	2.26	2.77	5.06	4.94
P_2O_5				0.12	0.15	0.11	0.16	0.15	0.12	0.14	0.15	0.14	0.15	0.27
Ce				89	60	71	132	80	99	134	37	55	102	91
Cr				181	242	393	296	229	198	303	198	252	298	240
Zn				95	91	148	111	59	94	154	16	47	79	42
Ba				909	652	748	893	774	844	526	432	523	652	1020
Nb				15	14	13	13	15	12	11	6	11	12	10
Rb				211	190	184	195	200	224	211	108	119	218	175
Sr				61	47	126	49	89	89	36	120	122	68	132
Y				32	23	23	23	30	26	28	21	20	28	30
LOI				2.26	2.04	1.30	2.82	1.87	2.58	1.37	1.27	1.51	1.82	2.41
Total	94.90	91.25	94.66	98.80	99.89	99.76	99.10	99.74	98.97	99.63	99.98	99.57	99.73	99.20
(Molecular proportions)														
SiO_2	71.40	71.61	69.89	69.70	76.91	74.02	68.76	72.53	70.37	67.33	82.76	80.51	70.78	72.43
Al_2O_3	11.59	11.70	11.44	12.96	9.69	10.53	13.01	11.46	12.96	16.31	7.27	8.43	11.44	13.85
$FeO^{\#}$	5.84	5.82	6.61	6.82	5.59	6.24	8.34	6.42	6.69	7.85	3.30	3.64	7.53	4.35
MgO	4.36	4.68	5.89	4.72	3.91	3.83	4.95	4.08	4.25	4.62	1.93	2.34	4.69	2.76
MnO		0.10	0.13	0.19	0.07	0.08	0.24	0.10	0.09	0.07	0.05	0.06	0.07	0.05
CaO	2.19	1.40	1.49	0.32	0.29	0.94	0.37	0.63	0.50	0.32	0.82	1.02	0.44	0.99
Na_2O	2.07	2.01	1.84	1.23	0.50	1.75	0.76	1.57	1.24	0.57	2.31	2.06	1.41	1.90
K_2O	2.55	2.70	2.71	4.06	3.05	2.62	3.56	3.21	3.89	2.93	1.56	1.94	3.66	3.67
X_{FeO}	0.57	0.55	0.52	0.58	0.58	0.61	0.62	0.61	0.61	0.63	0.62	0.60	0.61	0.61
X_{MnO}		0.010	0.010	0.016	0.007	0.007	0.018	0.010	0.009	0.005	0.009	0.009	0.006	0.007
X_{CaO}	0.51	0.41	0.45	0.21	0.37	0.35	0.33	0.29	0.29	0.36	0.26	0.33	0.24	0.34

Major elements reported in oxide wt.% with all Fe as FeO. Trace elements reported in ppm. Abbreviations of average pelite compositions: S; Shaw (1956), M; Mahar et al. (1997), and T; Tinkham et al. (2001). $X_{FeO}=FeO/(FeO+MgO+MnO)$, $X_{MnO}=MnO/(FeO+MgO+MnO)$, and $X_{CaO}= CaO/(CaO+Na_2O)$.
[#]All Fe as FeO.

the program PerPlex (Connolly, 1990). In all calculations, muscovite, quartz and water were assumed to be in excess. Mineral phases considered in the modeling include garnet, staurolite, biotite, chlorite, cordierite, chloritoid, zoisite and the aluminum silicate polymorphs, kyanite, sillimanite and andalusite. The compositions of garnet, staurolite, biotite, chlorite, cordierite, and chloritoid were allowed to vary along $FeMg_{-1}$, $FeMn_{-1}$ and $MnMg_{-1}$ solid–solution vectors. Tschermak substitutions, $AlAlSi_{-1}(Fe,Mg,Mn)_{-1}$, in biotite, chlorite, and muscovite were also considered. The thermodynamic dataset of Holland and Powell (1998) was used for the calculations except for aluminum silicates, which was based on Holland and Powell (1990). The Holland and Powell (1990) dataset gives a

location of the Al_2SiO_5 triple point close to that suggested by Pattison (1992), which is increasingly favoured in the literature (e.g., Spear et al., 1999; Cesare et al., 2003; Clarke et al., 2005). Solution models of Holland and Powell (1998) were used for garnet, staurolite, cordierite, chloritoid, chlorite, and muscovite. For plagioclase and biotite, the solution models of Newton et al. (1980) and Powell and Holland (1999), respectively, were employed.

P–T mineral assemblage stability diagrams ('pseudosections') are calculated for sub-aluminous sample B40 and aluminous sample D19 (Fig. 3a, b). Zoisite is not predicted to be stable in the bulk compositions anywhere in the *P–T* region of interest (450– 700 °C and 2–6 kbar). Chloritoid is predicted to be
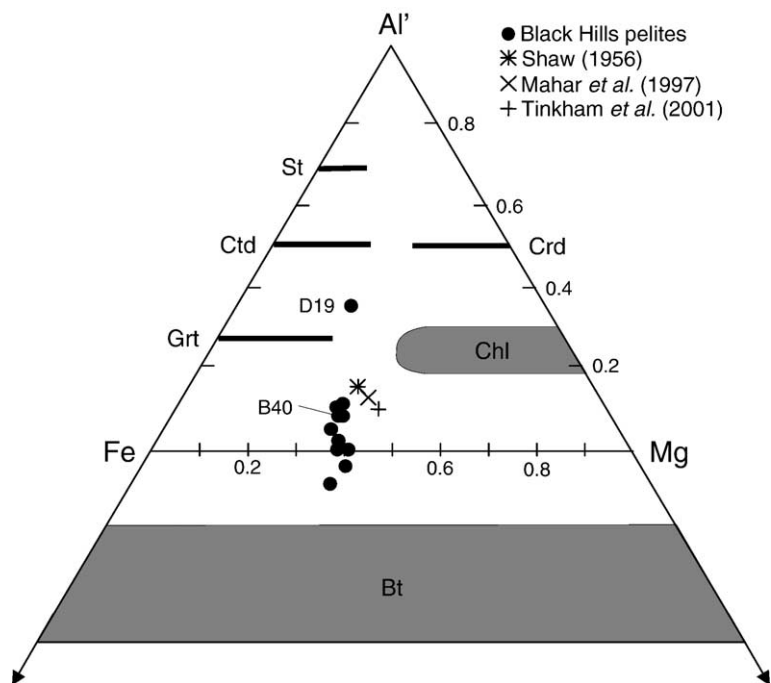
Fig. 2. Thompson (1957) AFM diagram illustrating the bulk-rock compositions projected from muscovite, albite, quartz, and H_2O. Average pelite compositions of Shaw (1956), Mahar et al. (1997), and Tinkham et al. (2001) are shown for comparison. Mineral and component abbreviations are from Kretz (1983).

stable only in the aluminous sample below the garnet zone (Fig. 3b). The stability of garnet-bearing assemblages is strongly controlled by Mn content in the pelites. In Mn-rich pelites, garnet occurs as an Mn-rich additional phase in many assemblages (e.g., Bt–Chl, St–Bt and And–Bt fields). The stability fields of Grt–St–Bt–Chl and Grt–Sil–St–Bt assemblages expand with increasing Mn contents in the bulk-rock. These
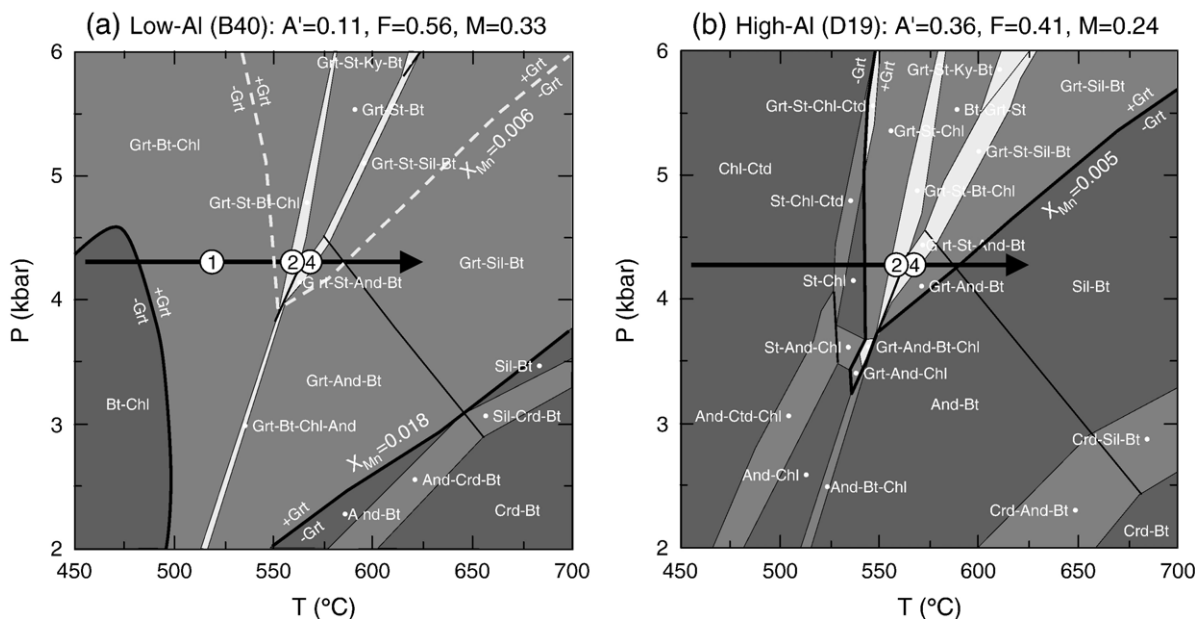
Fig. 3. *P–T* mineral assemblage diagrams for (a) sub-aluminous pelite B40 and (b) aluminous pelite D19. All assemblages include muscovite, plagioclase, quartz and H_2O. Numbers represent reactions discussed in the text. Note that stability of garnet expands with increasing bulk-rock Mn concentrations.

observations are consistent with previous studies on the addition of Mn to pelites (Spear and Cheney, 1989; Symmes and Ferry, 1992; Mahar et al., 1997; Tinkham et al., 2001).

The occurrence of coexisting staurolite and andalusite constrain metamorphic pressure in the area to about 4.3 kbar. This pressure estimation is sensitive to the position of the aluminum silicate triple point and is higher by about 0.5 kbar than estimated for other facies 2b settings (Pattison and Tracy, 1991). The estimated metamorphic pressure overlaps with the high end of the range of the pressure estimations (2.0–4.4 kbar) of Helms and Labotka (1991). The absolute pressure is not critical to the interpretations below. Along the isobaric heating path, the following series of prograde metamorphic reactions are predicted for the sub-aluminous bulk compositions (reaction numbers plotted on Fig. 3). Garnet starts to crystallize by the reaction:

$$Chl + Ms + Qtz = Grt + Bt + H_2O. \qquad (1)$$

at the staurolite isograd, consumption of garnet follows by the reaction:

$$Grt + Chl + Ms + Qtz = St + Bt + H_2O. \qquad (2)$$
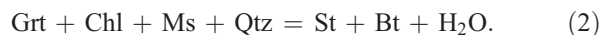
When chlorite is completely consumed, garnet resumes growth by the reaction:

$$St + Bt + Qtz = Grt + Ms + H_2O \qquad (3)$$

with further growth of garnet at the andalusite isograd by the reaction:

$$St + Ms + Qtz = Bt + Grt + And + H_2O. \qquad (4)$$

After the breakdown of staurolite, garnet is predicted to undergo resorption by the reaction:

$$Grt + Ms + Qtz = And + Bt + H_2O \qquad (5)$$
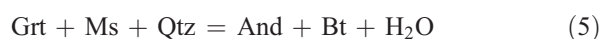
followed by the andalusite–sillimanite transition reaction

$$And = Sil. \qquad (6)$$

Further resorption of garnet is predicted by the reaction,

$$Grt + Ms + Qtz = Sil + Bt + H_2O. \qquad (7)$$

In the aluminous pelite D19, biotite first appears with staurolite at much higher temperature than in the sub-aluminous pelites, and the Grt–St–Bt–Chl assemblage is preceded by a biotite-free Grt–St–Chl assemblage (Fig. 3b). The rest of the reaction sequence after garnet consumption at the staurolite isograd (reaction 2) is the same as for the sub-aluminous pelites. It is important to note that in both the sub-aluminous and aluminous pelites, garnet is predicted to undergo first resorption at the staurolite isograd, re-growth at the andalusite isograd, and a second episode of resorption after the breakdown of staurolite along the isobaric heating path.

The predicted changes in mineral modes along the isobaric heating path in the sub-aluminous pelite B40 and aluminous pelite D19 are shown in Fig. 4a and b, respectively. Crystallization of staurolite and biotite cause the most dramatic changes in mineral modes in sub-aluminous and aluminous pelites, respectively. In the staurolite zone, garnet in aluminous sample D19 is predicted to experience more volume loss (84%) than that in sub-aluminous sample B40 (35%). These volume changes in the major silicates at the staurolite isograd can influence trace element budgets in the rocks because of their relatively large volume compared to accessory phases, even if their trace elements are present only at a several ppm level.

The effects of bulk-rock Al_2O_3 on the phase relations and degree of garnet resorption at the staurolite isograd reaction are shown in a $T–X_{Al}$ diagram (Fig. 5). In the $T–X_{Al}$ diagram, bulk Al_2O_3 concentrations were allowed to vary from 22 to 40 wt.%, encompassing the ranges of Al_2O_3 content of samples B40 and D19. The addition of Al_2O_3 to the original bulk composition of B40 was done by proportional reduction of the other elements. At a constant pressure, the stability field of Grt–St–Bt–Chl is a function of bulk-rock Al content, with a maximum located at the boundary between the sub-aluminous and aluminous pelites. The patterns of the contours of garnet modal abundance in the areas between staurolite and andalusite zones confirm more consumption of garnet in aluminous pelites (Fig. 5).

4.3. Chemical zoning of garnet

Black Hills garnet porphyroblasts are post-tectonic, overgrowing the predominant foliation (S_2). Representative photomicrographs of garnet porphyroblasts co-existing with staurolite are shown in Fig. 6. In contrast to the 35% resorption of garnet predicted in the staurolite zone, garnet porphyroblasts from sub-aluminous pelites (B40, A43, and B56) show no clear textural evidence of resorption (Fig. 6b, c). In contrast to garnet in the sub-aluminous pelites, garnet porphyroblasts from the aluminous pelite D19 are partially replaced
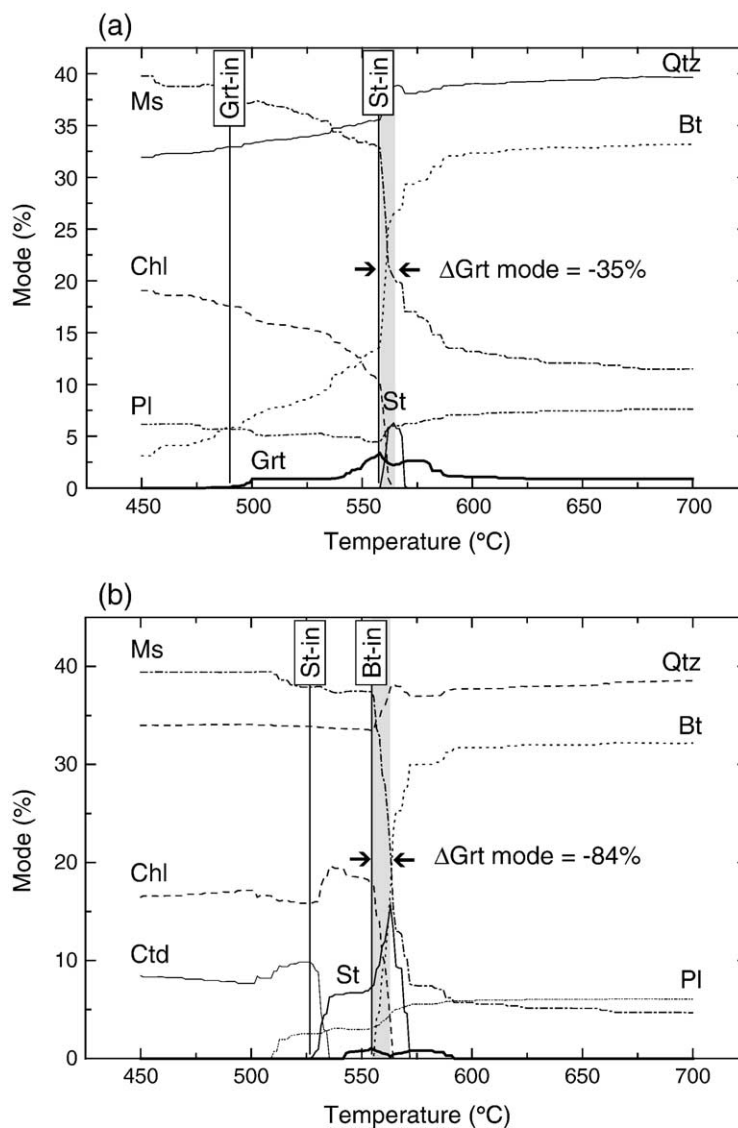
Fig. 4. Diagrams showing variations of mineral modes (%) along an isobaric heating path at 4.3 kbar calculated for (a) sub-aluminous pelite B40 and (b) aluminous pelite D19. Note that the percent volume loss of garnet at the shaded areas is smaller in the sub-aluminous pelite compared to the aluminous pelite.

by biotite (Fig. 6d), compatible with the predicted higher resorption (83%) than sub-aluminous pelites. The biotite selvage preserves the original shape of the former euhedral garnet porphyroblasts.

Of the twelve samples selected for this study, the garnet in five samples displayed Y annuli, and the garnet in the other seven did not. X-ray maps of the garnet from the five samples in which Y annuli were found are presented in Fig. 7. Rim–core–rim zoning profiles of the five garnet porphyroblasts are given in Fig. 8. In garnet D31 from the garnet zone, Y decreases gradually from the core towards the rim before increasing at the outermost rim (Figs. 7a and 8a), producing

an annulus of 300 μm width. In this garnet, inclusions are abundant in the core and relatively absent in the Y-rich rim.

Garnet B40 is characterized by a euhedral, high-Y (~5200 ppm) core (Figs. 7d and 8b). In another garnet with a similar Y-rich core, xenotime was found as inclusions, suggesting that the high-Y core of the garnet grew at the expense of xenotime. YAG-xenotime geothermometer (Pyle and Spear, 2000) applied to the core of garnet B40 results in a temperature of 462 °C, close to ~480 °C for the onset of garnet at 4.3 kbar (Fig. 3a) and suggestive of equilibration between garnet and xenotime. Beyond the high-Y zone in B40, Y concen-
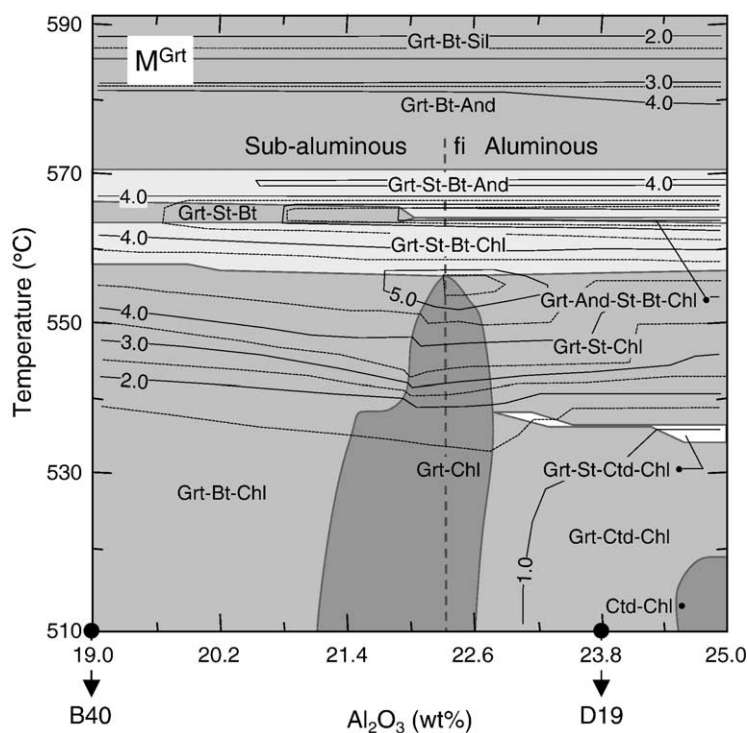
Fig. 5. A $T–X_{Al}$ section with contours of garnet volume calculated at 4.3 kbar for bulk Al_2O_3 contents encompassing those of sub-aluminous pelite B40 and aluminous pelite D19. All assemblages include muscovite, plagioclase, quartz and H_2O. Note that aluminous pelites are predicted to experience more garnet consumption in the staurolite zone than sub-aluminous pelites.

tration drops sharply to 400 ppm, consistent with growth in the absence of xenotime (Pyle and Spear, 1999). Y then increases again to 890 ppm, forming a thin euhedral annulus (30 μm) closely following the crystal outline, before dropping to below the detection limit (~100 ppm). Unlike garnet D31 from the garnet zone, garnet B40 shows overgrowth after the formation of the Y annulus. Similar Y annuli outboard of the high-Y cores also occur in euhedral garnet inclusions in staurolite in the same rock, suggesting that the annuli were produced before cessation of growth of staurolite in the pelite.

Garnet A43 from the andalusite zone displays a euhedral but discontinuous Y annulus obscured by numerous inclusions (Figs. 7g and 8c). Unlike the Y annulus in garnet D31, the Y annulus in garnet A43 is located within the inclusion-rich area. Inclusions in garnet A43 include quartz, biotite, ilmenite, rutile, apatite, and monazite. Among the inclusions, monazite is the only one occurring exclusively outside of the Y annulus, implying that crystallization of monazite may be related to the formation of the Y annulus in the garnet.

Yttrium in garnet D19 from the andalusite zone initially increases outward, producing a relatively

thick (200 μm width) annulus that has been partially truncated by the biotite selvage (Figs. 7j and 8d). Resorption of Y-rich garnet resulted in the production of xenotime in the biotite selvage, such as reported by Pyle and Spear (1999). In sample D19, following the resorption, garnet appears to have grown further by the andalusite-forming reaction (4) in equilibrium with xenotime, as indicated by the thin continuous low-Y, low-Ca rim around the truncated garnet (Fig. 7j).

Garnet A5 from the sillimanite zone shows a similar Y zoning pattern to garnet D19 from andalusite zone (Figs. 7m and 8e), namely a low-Y core with a relatively thick (120 μm) Y annulus midway between the core and rim. However, the Y annulus of garnet A5 is not truncated by resorption as in garnet D19.

Manganese zoning of garnet from the garnet, staurolite, and lower andalusite zones (D31, B40, A43) are typical of garnets in low to medium grade metapelites, characterized by the high-Mn in the core with gradually decreasing Mn toward the rim (Fig. 8a–c). In contrast to the euhedral zoning patterns of Y preserved in garnets B40 and A43, Mn zoning in the two garnet porphyroblasts is rounded at the corners of the crystals (Fig. 7e, h), suggesting faster volume diffusion of Mn than Y as reported by Chernoff and Carlson (1997, 1999).
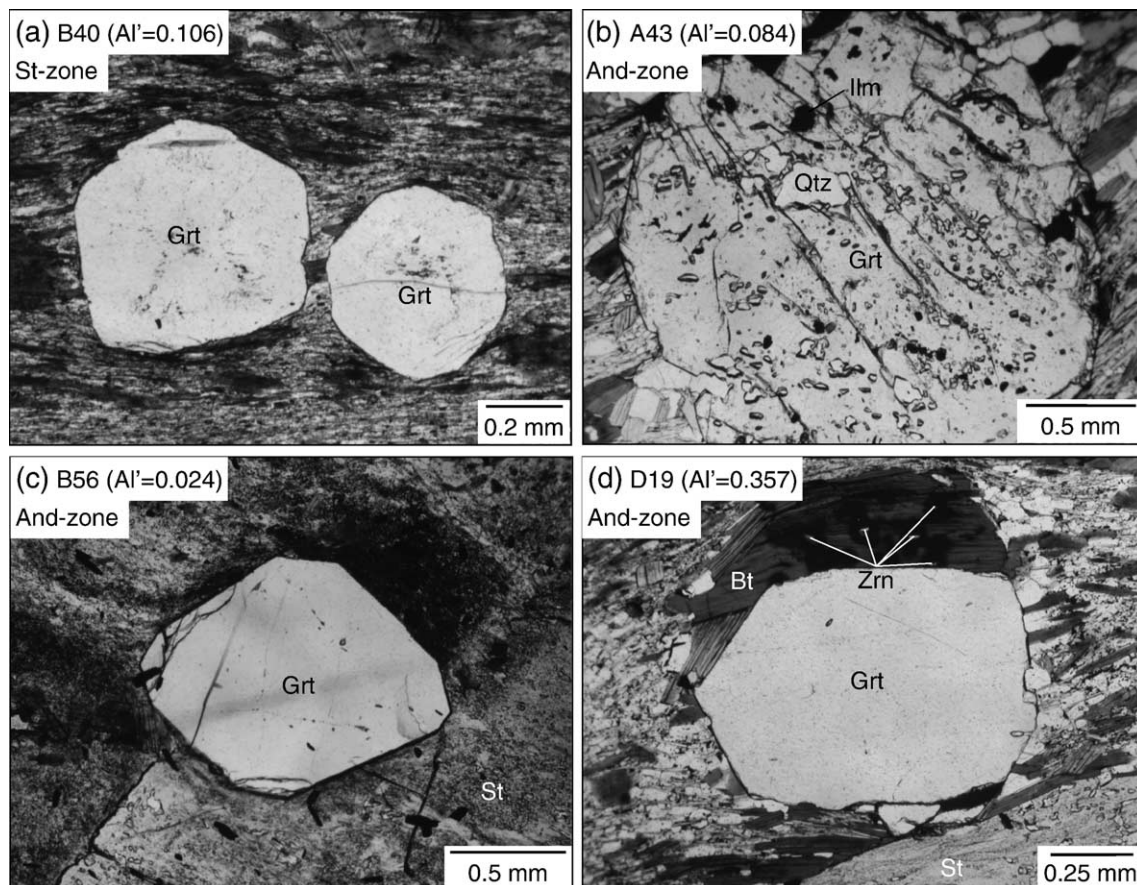
Fig. 6. Photomicrographs of garnets coexisting with staurolite in sub-aluminous pelites (a) B40, (b) A43, and (c) B56 and aluminous pelite (d) D19. Projected Al′ values are given on the microphotographs. Note the biotite selvages in the aluminous pelite D19.

Mn zoning becomes homogenized in the upper andalusite and sillimanite zones, resulting in flat zoning profiles in the cores with localized enrichment at the rims of garnets D19 and A5 (Fig. 8d, e). A narrow zone of increasing Mn towards the rim is interpreted to be due to back diffusion during resorption. The increase in Mn, however, is not accompanied by an increase in Y, indicating that Y released during garnet resorption did not diffuse back into the garnet.

Black Hills garnets display variable Ca zoning. Garnet D31 shows a core slightly enriched in Ca (Fig. 7c). In sample B40, garnet has a high-Ca core with an inflection midway between core and rim (Fig. 7f), the location of which is not coincident with that of the Y annulus in the garnet. Garnet A43 shows irregular Ca zoning in the inclusion-rich core and a thin (~90 μm) Ca-depleted zone in the inclusion-free rim (Fig. 7i). Garnet D19 displays a slightly low-Ca core with sector zoned intermediate area, surrounded by a thin (<50 μm) discontinuous Ca-depleted rim (Fig. 7l). The sector zoned Ca zoning is correlated exactly with the relative-

ly broad Y annulus in the garnet. Although a Ca-depleted rim occurs at the similar location with the Mn-enriched rim in garnet D19 (Fig. 7k, l), they are unlikely to be genetically correlated because the low-Ca rim which also occurs in garnet A43 is interpreted to be a growth feature and the high-Mn rim is most likely a retrograde feature. This interpretation is in consistent with the wider low-Ca rim than Mn-enriched rim in the garnet D19. Garnet A5 has a low-Ca core with an inflection at the location of the Y annulus (Fig. 7o).

The inflections in Ca zoning observed in garnets B40, D19, and A5 are not compatible with the predicted equilibrium growth of garnet along an isobaric heating path in pelitic rocks (e.g., Figs. 3 and 4), because Ca is predicted to decrease continuously from core to rim with no inflections (Spear et al., 1990; Vance and Mahar, 1998; this study). The inflections in Ca zoning, therefore, indicate either disequilibrium partitioning of Ca or reflect the former presence of other calcic minerals other than garnet and plagioclase that were not observed at the peak mineral assemblages. The irregular
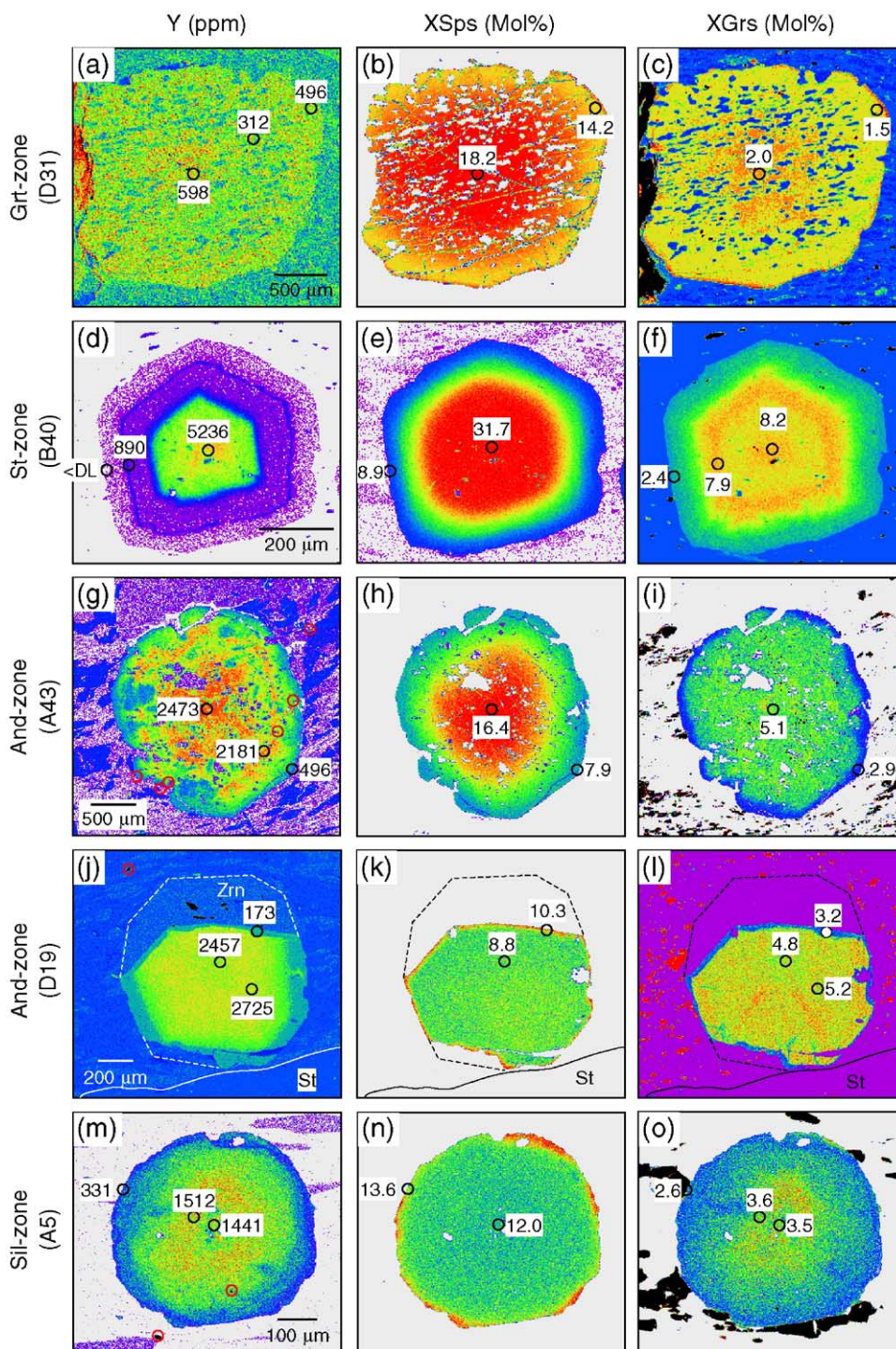
Fig. 7. Digital elemental X-ray maps of Y, X_{Sps}, and X_{Grs} in garnets (a–c) D31, (d–f) B40, (g–i) A43, (j–l) D19, and (m–o) A5. Representative spot analyses are marked as black circles in the images. The locations of monazite grains are given as red circles. Dashed lines in the X-ray maps of garnet D19 represent the margin of former garnet porphyroblast. Warm colors represent higher elemental concentrations.

zoning in the inclusion-rich core of garnet A43 and sector zoning in garnet D19 suggest disequilibrium partitioning of Ca, which is not recorded by Mn and Y in the garnet. If this is true, then the low-Ca rims of garnets A43 and D19 may represent equilibrium Ca compositions achieved at higher temperatures.
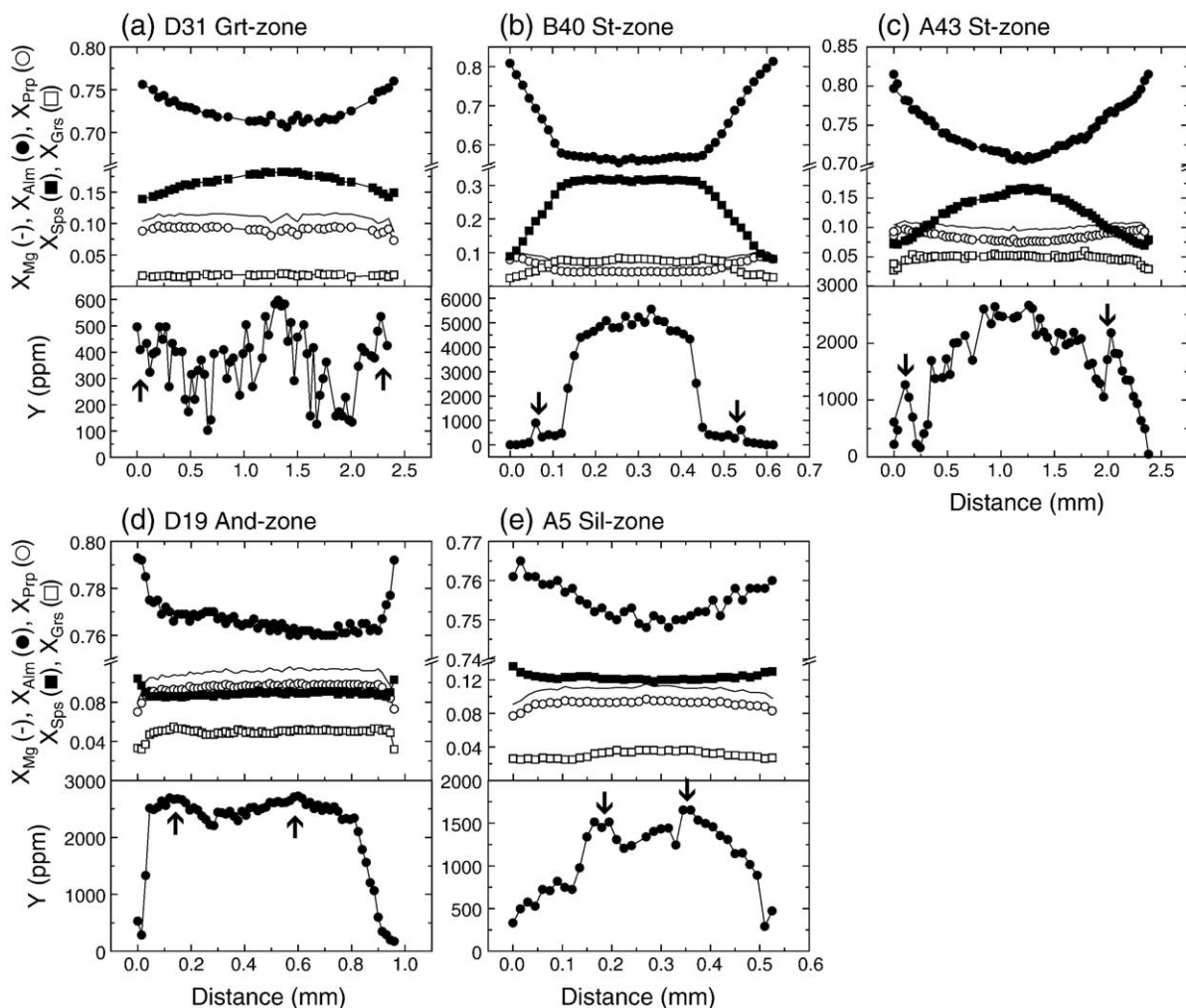
Fig. 8. Rim-to-rim zoning profiles of garnet from Black Hills. The locations of Y-annuli are indicated by arrows on Y zoning profiles.

4.4. Chemical zoning of monazite

Representative Th, U and Y maps of monazite from garnet to sillimanite zones are presented in Fig. 9. X-ray mapped monazite grains occur in the matrix except for monazite B40 included in a garnet which is, in turn, included in staurolite. Zoning patterns of the monazite inclusions are similar to those of matrix monazite in the same rock.

Thorium zoning in monazite shows two different patterns that correlate with the different types of Y zoning in coexisting garnet. Monazite grains coexisting with garnet with no Y annuli display a high-Th core with a concentrically decreasing zoning pattern towards the rim (Fig. 9a, c, f, h, i). In contrast, monazite grains coexisting with garnet with Y annuli show irregular zoning patterns with multiple high-Th domains (Fig. 9b, d, e, g, j), suggestive of pseudomorphous replace-

ment of pre-existing minerals or overgrowth of a heterogeneous matrix (Yang and Rivers, 2001; Carlson, 2002; Hirsch et al., 2003). Overprint zoning on a heterogeneous matrix, however, is not likely the primary reason because the irregular zoning would be expected in all samples, not just those containing garnet with Y annuli. Pseudomorphous replacement of allanite by monazite is commonly reported in upper greenschist facies pelitic rocks (Wing et al., 2003; Fraser et al., 2004; Tomkins and Pattison, 2005).

Monazite grains from the garnet and staurolite zones are not significantly zoned in U and Y. In the andalusite zone, monazite grains display similar U and Y zoning as those of lower grade when garnet is not resorbed (A43 and B56). When garnet D19 from the upper andalusite zone experiences resorption at the staurolite zone, monazite grains show Y-enriched rims. Monazite grains from the sillimanite zone, however, display distinctive
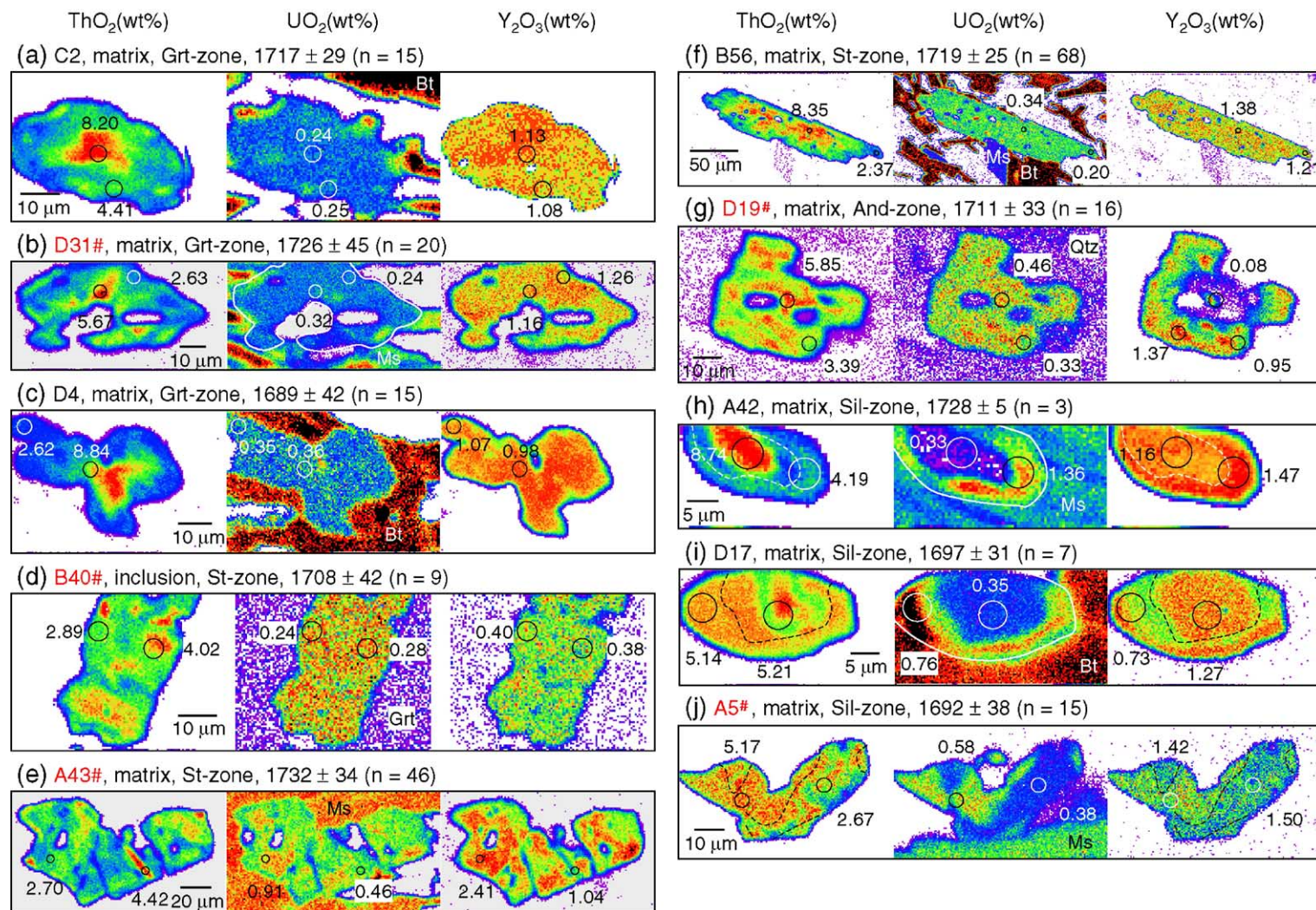
Fig. 9. Digital elemental X-ray maps of Th, U, and Y in Black Hills monazite with average chemical ages for selected samples. Representative spot analyses are given as open circles. Pelites containing garnet with Y-annuli are labeled in red. Warm colors represent higher elemental concentrations.

Table 4
Representative age analyses of monazite from Black Hills

	D31 (Grt-zone)			B40 (St-zone)			B53 (St-zone)			B56 (St-zone)		
	L-Th	M-Th	H-Th	L-Th	M-Th	H-Th	L-Th	M-Th	H-Th	L-Th	M-Th	H-Th
	mx	mx	mx	inc	inc	inc	mx	mx	mx	mx	mx	mx
P_2O_5	31.08	31.02	30.60	18.96	28.95	28.92	31.16	30.17	29.89	30.97	30.86	30.13
Ce_2O_3	31.24	30.76	28.55	17.48	28.85	27.15	31.04	29.43	27.05	30.57	28.85	27.49
La_2O_3	16.13	15.81	14.66	7.75	14.44	12.96	16.49	15.83	14.57	16.03	14.98	14.30
Y_2O_3	1.14	1.09	1.16	0.27	0.36	0.25	1.09	1.06	1.10	1.21	1.30	1.32
ThO_2	1.95	2.64	5.67	1.39	3.85	9.96	2.02	4.12	8.82	3.06	5.41	7.80
UO_2	0.21	0.21	0.28	0.16	0.20	0.25	0.18	0.20	0.15	0.18	0.23	0.26
PbO	0.20	0.26	0.50	0.15	0.34	0.81	0.20	0.36	0.70	0.28	0.46	0.65
Age (Ma)	1684	1720	1690	1712	1693	1708	1669	1705	1706	1702	1686	1693
Error[#]	60	50	28	80	43	23	62	36	23	46	30	23

	A43 (St-zone)			D19 (And-zone)			D17 (Sil-zone)			D17 (Sil-zone)		
	L-Th	M-Th	H-Th	L-Th	M-Th	H-Th	L-Th	M-Th	H-Th	L-Th	M-Th	H-Th
	mx	mx	mx	mx	mx	mx	mx	mx	mx	mx	mx	mx
P_2O_5	30.79	31.03	30.52	30.62	29.99	30.38	30.74	30.70	30.56	31.24	30.92	30.70
Ce_2O_3	29.38	28.80	27.30	29.48	27.16	28.88	29.63	29.42	28.63	31.15	30.21	28.16
La_2O_3	15.02	14.65	14.12	15.44	14.04	15.76	15.40	15.18	14.74	15.55	15.14	14.24
Y_2O_3	2.17	2.29	1.58	0.95	1.18	0.08	1.19	1.17	1.22	1.38	1.29	1.36
ThO_2	2.24	2.87	5.84	3.39	4.37	5.85	3.89	4.82	5.77	2.22	3.80	5.47
UO_2	0.77	0.56	0.45	0.31	0.60	0.42	0.33	0.29	0.32	0.27	0.27	0.37
PbO	0.38	0.37	0.56	0.34	0.48	0.56	0.38	0.44	0.51	0.24	0.37	0.51
Age (Ma)	1721	1717	1695	1715	1678	1716	1701	1704	1687	1719	1746	1713
Error[#]	38	40	32	44	31	29	40	36	31	58	42	28

[#]Errors calculated at one sigma on the basis of counting statistics of Th, U, and Pb.

Abbreviation: L-Th: low-Th, M-Th: medium-Th, H-Th: high-Th, mx: matrix monazite, inc: monazite inclusions in garnet. Unanalyzed oxides are treated as Nd_2O_3.

increases in both U and Y at the rims outboard of the low-U cores from the lower grades, regardless of Y-zoning patterns in coexisting garnet porphyroblasts (Fig. 9g–j). Th and Y zoning in the low-U cores of sillimanite zone monazite show the same patterns as monazite from the garnet and staurolite zones: single high-Th core in monazites A42 and D17 coexisting with garnet with continuous Y zoning, and irregular Th zoning in monazite A5 coexisting with garnet with Y annuli (Fig. 9h–j). This suggests that the monazite cores formed at lower grades and persisted into the sillimanite zone. The homogeneous low-U and -Y cores of sillimanite zone monazite are defined as monazite 1 and the U- and Y-rich rims are defined as monazite 2.

4.5. Chemical ages of monazite

Representative electron microprobe ages of Black Hills monazite are given in Table 4 and summarized in Table 5 according to their textural locations, generations, and chemical domains. Ages influenced by inclusions, especially in the cores, and edge effects at the rims of monazite grains have been removed from the data set on the basis of P_2O_5 contents. Although X-ray mapping of Th shows significant core to rim zoning in monazite, chemical ages in both Th-rich cores and Th-poor rims of the grains show similar ages within 1σ standard deviations (Table 5). Electron microprobe ages of the monazite 1 overlap with monazite 2 in the

Table 5
Summary of chemical ages of monazite in the Black Hills pelites

		Th zoning		Textural locations		Generations	
	All	High-Th	Low-Th	Inclusions	Matrix	First	Second
Average (Ma)	1713	1709	1714	1713	1713	1712	1713
Standard deviation (1σ)	39	34	40	39	39	39	38
Standard errors (2σ)	4	7	5	13	4	4	20
Number	343	83	260	36	307	317	15
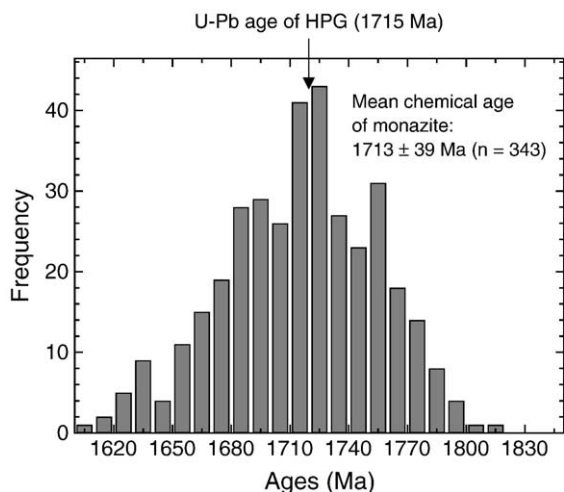
Fig. 10. Distributions of the chemical ages in monazite from Black Hills pelites showing a peak at around 1713 Ma. Total number of spot analyses is 343 from 22 grains in 12 samples.

sillimanite zone. There is no significant difference in age between monazite included in garnet and matrix monazite, suggesting that garnet porphyroblasts were produced by the thermal metamorphism related to the intrusion of the HPG. The average monazite age of 343 points on 22 grains from 12 samples is 1713 ± 39 Ma (Table 5), close to the intrusion age of the HPG obtained from U–Pb dating of monazite (1715 ± 3 Ma, Redden et al., 1990). The age histogram shows ages ranging from 1650 to 1800 with a peak centered around the granite intrusion age (Fig. 10). Within the

resolution of electron microprobe dating technique, therefore, this indicates a single thermal event in the contact aureole. In conjunction with ion microprobe analyses, Dahl et al. (2005), however, reported two different electron microprobe ages at ~1755 and ~1715 Ma between core and rim domains in monazite grains mainly from Bear Mountain gneiss dome located 10 km west of the study area.

4.6. Bulk-rock X_{Ca} vs. Al ratios

In the chemical system considered in this study, NCMnKFMASH, the most variable components in the Black Hills rocks are Na_2O, CaO and Al_2O_3 (Table 3). X_{Ca} [$=Ca/(Ca+Na)$] values are plotted against Al′ numbers in Fig. 11, together with the average pelites of Shaw (1956), Mahar et al. (1997) and Tinkham et al. (2001). The Black Hills pelites are less calcic than the three average pelites and can be divided into two groups in terms of bulk-rock X_{Ca} and Y zoning in garnet. Pelites with Y annuli in garnet are systematically more calcic than pelites with no Y annuli in garnet, except for sample D17 which has unusually high P_2O_5 content (Table 3). The occurrence of Y annuli in garnet and irregular Th zoning in monazite in samples with bulk-rock X_{Ca} ratios larger than 0.18 suggests the original presence of Y-bearing calcic minerals in the pelites, such as epidote and allanite. The role of Al′ values in sample discrimination appears to be less significant.
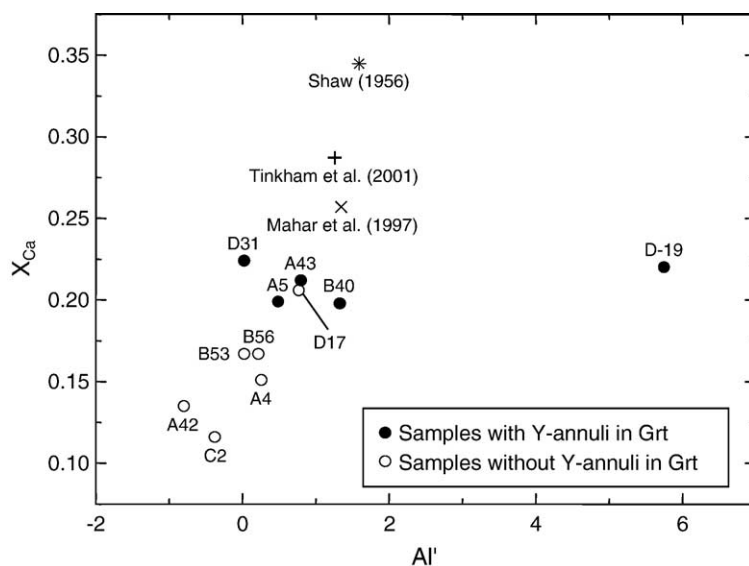
Fig. 11. Bulk-rock X_{Ca} [$=Ca/(Ca+Na)$] vs. Al′ diagram showing discrimination between pelites with Y-annuli in garnet and pelites without Y-annuli in garnet. Average bulk-rock compositions of Shaw (1956), Mahar et al. (1997), and Tinkham et al. (2001) are also given for references.

5. Discussion and conclusions

5.1. The origin of Y annuli in black hills garnet

Understanding the origin of Y annuli in garnet from pelitic rocks is important because the annuli signal discontinuous events that may include breakdown of Y-rich mineral phases, resorption-and-regrowth of garnet, fluid infiltration, and changes in garnet growth rates. Possibilities of these processes are discussed below.

5.1.1. Breakdown of Y-enriched phases

Discontinuous breakdown of Y-rich mineral phases such as epidote and allanite has been suggested for the origin of Y annuli in garnet from calc-pelites (e.g., Hickmott et al., 1987; Hickmott and Spear, 1992). Known Y-rich accessory minerals in the Black Hills pelites are xenotime, zircon, monazite, and apatite. Among them, the breakdown of xenotime is the most effective method by which to increase the availability of Y in the rock. However, xenotime buffers the Y abundance in coexisting minerals at a high level until it disappears, so that breakdown of xenotime results in an abrupt decrease in Y rather than an annulus (Pyle and Spear, 1999, 2003). This step-like Y zoning is observed in garnet B40 of this study. The Y annulus in garnet B40 occurs outboard of the high-Y domain (Fig. 7d), indicating that the Y annulus forming event occurred after the breakdown of xenotime. The presence of the Y annuli in garnet included in staurolite provides another constraint on the time of Y annuli formation as before the cessation of the growth of staurolite. Together with the occurrence of the Y annuli in garnet zone, it is concluded that the Y annuli were formed in the garnet zone.

Other accessory minerals such as zircon, monazite, and apatite, while not saturated in Y, can incorporate significant amounts of Y (e.g., Heinrich et al., 1997; Finger et al., 1998; McFarlane et al., 2005) and thus have a pronounced effect on Y fractionation. Among them, zircon and apatite occur at all grades as both inclusions in garnet and matrix minerals. Monazite occurs as inclusions in garnet but only outside of the Y annuli, implying that it may be related to the Y annuli forming event.

The restriction of garnet with Y annuli to relatively calcic pelites (Fig. 11) suggests a link between the Y annuli and Y-rich calcic phases. The inflections in Ca zoning in garnet porphyroblasts B40, D19 and A5 (Fig. 7f, l, o) also suggest that there were calcic minerals such as calcite, allanite and epidote involved in the formation of garnet. Among the three minerals, calcite does not contribute to the budgets of Y and LREE in the rocks. The breakdown of epidote is expected to produce abrupt decreases in Ca (Menard and Spear, 1993) at the locations of the Y annuli, rather than discontinuous increases. Thus, even though it has not been found in the Black Hills pelites, we are left with allanite as the most likely control on Y zoning in garnet and as the most likely precursor LREE mineral to monazite.

The irregular chemical zoning observed in monazite coexisting with garnet with Y annuli is consistent with pseudomorphous replacement of allanite. Pseudomorphous replacement is generally favoured in environments where intergranular diffusion is less efficient than volume diffusion (Ferry, 2000; Carlson, 2002). Natural examples of limited integranular diffusion include 'overprint zoning' in garnet for sluggish elements such as Mn and Cr described by Hirsch et al. (2003) and Yang and Rivers (2001), respectively. They demonstrated that intergranular diffusion of Mn and Cr in medium grade metamorphic rocks was slow enough that garnet crystals, as they grew, incorporated heterogeneity in the matrix from which they formed.

Wing et al. (2003) suggested that metamorphic allanite disappeared at the andalusite isograd to produce monazite in the Waterville Formation, NW Maine. They showed that bulk-rock CaO and Al_2O_3 contents exerted a significant control on the allanite–monazite transition in these schists, with the transition occurring at higher grade in more calcic and aluminous pelites. The presence of monazite and absence of allanite in garnet and staurolite zone samples from the Black Hills and the occurrence of Y annuli between core and rim of garnet from the garnet and staurolite zones, indicate that the allanite–monazite transition occurs in the garnet zone.

5.1.2. Resorption of garnet

Yttrium-annuli in garnet from pelitic rocks have been attributed to the resorption of garnet at the staurolite zone followed by regrowth later at higher grade (Pyle and Spear, 1999; Kohn and Malloy, 2004). The distribution and characteristics of Y annuli in Black Hills garnets, however, are not compatible with the resorption-and-regrowth model for the following reasons: (1) the occurrence of Y annuli in garnet from the garnet zone, (2) the euhedral shape of the Y annuli, with little to no evidence for embayments, rounding of crystal corners, or other features that normally accompanying resorption, (3) the occurrence of Y annuli in both matrix garnet and garnet included in staurolite porphyroblasts, (4) the absence of Y annuli in some garnet

porphyroblasts coexisting with staurolite, and (5) the significant overgrowth of garnet rims after the formation of Y annuli in garnet from the staurolite zone.

Garnet D19, the only garnet showing evidence of resorption-and-regrowth, provides some constraints on the conditions of Y annuli formation in garnet. In garnet D19, there are no Y annuli developed at the interfaces between resorption and regrowth because of the xenotime in the biotite selvages. Resorption of Y-rich garnet cores in the staurolite zone releases Y into the matrix stabilizing xenotime (Pyle and Spear, 1999). When garnet D19 grew again in the andalusite zone, the level of Y was buffered by the xenotime, resulting in the thin homogeneous Y-poor rim coinciding with the Ca-poor rim.

The resorption of garnet in the staurolite zone has been considered as the reaction responsible for first major growth of monazite in many studies (e.g., Smith and Barreiro, 1990; Pyle and Spear, 1999; Kohn and Malloy, 2004). Excluding apatite and other LREE-minerals, modes of monazite that could have

been produced by the breakdown of major silicates at the staurolite-isograd are calculated in Table 6. Since P is not a limiting factor in the growth of monazite (Kohn and Malloy, 2004), the mass-balance calculations were done on LREE using LREE compositions reported for major minerals in other metamorphic rocks (Bea et al., 1994; Bea, 1996; Bea and Montero, 1999; Yang et al., 1999; Yang and Rivers, 2000, 2002). Modes of the major minerals before and after the staurolite-isograd reaction were estimated from the $P-T$ mineral assemblage modeling. Specific gravity data for the mineral phases are from Deer et al. (1992). Most monazites contain approximately 50 wt.% LREE. Measured modes of monazite in samples B40 and D19 were 0.019% and 0.022%, respectively.

The maximum mode of monazite that can be produced by the staurolite-isograd reaction is less than 3% of monazite observed in the rocks (Table 6). The mode of monazite would be even smaller if LREE in product minerals such as plagioclase and biotite are considered. This result suggests that the major phases involved in

Table 6
Mass balance calculations for LREE in sample B40 and D19

Minerals	Mode[i] (%)	Mode[f] (%)	LREE (ppm)	SG	Contribution[i] (ppm) min	Contribution[i] (ppm) max	Contribution[f] (ppm) min	Contribution[f] (ppm) max
B40: staurolite-zone								
Grt	3.35	2.19	0	3.921	0.00	0.00	0.00	0.00
Chl	10.18	0.00	1–5	2.950	0.12	0.62	0.00	0.00
Ms	32.85	20.32	2–20	2.825	0.77	7.68	0.47	4.67
Pl	4.45	5.99	5–50	2.690	0.25	2.48	0.33	3.28
St	0.04	6.26	0	3.785	0.00	0.00	0.00	0.00
Bt	13.58	26.48	1–10	3.000	0.17	1.69	0.32	3.23
Qtz	35.56	38.76	0	2.650	0.00	0.00	0.00	0.00
Total	100	100	9–85		1.31	12.47	1.12	11.18
Released LREE (ppm)							0.43	3.63
Calculated mode of monazite (%)							0.00004	0.00038
Measured mode of monazite (%)							0.019	0.019
% of calculated monazite relative to the measured monazite							0.23	1.99
D19: andalusite-zone								
Grt	1.04	0.17	0	3.921	0.000	0.000	0.000	0.000
Chl	17.75	3.59	1–5	2.950	0.214	1.070	0.042	0.211
Ms	37.42	21.07	2–20	2.825	0.864	8.642	0.475	4.746
Pl	3.06	4.59	5–50	2.690	0.168	1.680	0.246	2.463
St	7.27	15.59	0	3.785	0.000	0.000	0.000	0.000
Bt	0.00	17.16	1–10	3.000	0.000	0.000	0.205	2.052
Qtz	33.46	37.83	0	2.650	0.000	0.000	0.000	0.000
Total	100	100	9–85		1.246	11.392	0.968	9.471
Released LREE (ppm)							0.56	4.76
Calculated mode of monazite (%)							0.00006	0.00050
Measured mode of monazite (%)							0.022	0.022
% of calculated monazite relative to the measured monazite							0.27	2.29

Superscripts i and f represent before and after the staurolite-isograd reaction, respectively. SG represents for specific gravity from Deer et al. (1992). Modes were estimated from the $P-T$ mineral assemblage modeling. LREE contents of minerals are based on the laser-ablation ICP-MS analyses of metamorphic rocks (Bea et al., 1994; Bea, 1996; Bea and Montero, 1999; Yang et al., 1999, Yang and Rivers, 2000, 2002).

the staurolite-isograd reaction are not responsible for the major growth of monazite, and that consumption of a LREE accessory mineral (e.g., allanite and LREE oxides) was primarily responsible for monazite growth. This result also implies that once monazite forms at the expense of the precursor LREE-rich mineral, it does not undergo any further significant growth by reactions involving major silicate minerals alone. Therefore, the most likely source of additional LREE for the growth of monazite 2 after the breakdown of allanite is monazite 1.

5.1.3. Y-rich fluid infiltration

In addition to bulk partition coefficient changes effected by discontinuous breakdown of Y-rich minerals such as xenotime and allanite, introduction of external Y-rich fluids into the pelites could produce the observed Y annuli. Numerous trace element-rich, including REE, pegmatites occur around the HPG (Duke et al., 1988; Shearer et al., 1992). Although it is possible that REE-rich metasomatic fluids interacted with the pelites of the Black Hills, the occurrence of Y annuli in garnet from regional metamorphic settings with no apparent association with igneous activities (Pyle and Spear, 1999, 2000; Yang and Rivers, 2002; Kohn and Malloy, 2004) suggests that an internal control is more likely.

5.1.4. Changes in garnet growth rates

Due to the strong compatibility of Y in garnet, a decrease in garnet growth rate results in an increase in Y concentration at growing garnet–matrix interface if the inter-granular diffusion of Y is limited (Hickmott et al., 1987; Hickmott and Spear, 1992; Schwandt et al., 1996). Assuming the density of inclusions in garnet reflect changes in garnet growth rates, the increase of Y at the inclusion-poor rim of garnet D31 (Fig. 7a) could be compatible with changes in garnet growth rates. However, the occurrence of the Y annulus in garnet A43 within the inclusion-packed core (Fig. 7g), suggests that the formation of the Y annulus is not related to the changes in garnet growth rates. If changes in garnet growth rate were the primary cause of the observed Y annuli then we might predict that we should observe decoupled behaviour between garnet compatible and incompatible elements such as Mn and Ca, which is not observed.

5.2. Paragenesis of xenotime, allanite and monazite

Our preferred interpretation of the paragenesis of xenotime, monazite, and allanite in relation to garnet B40 is summarized in Fig. 12. The initial growth of garnet at point 1 was in equilibrium with xenotime as
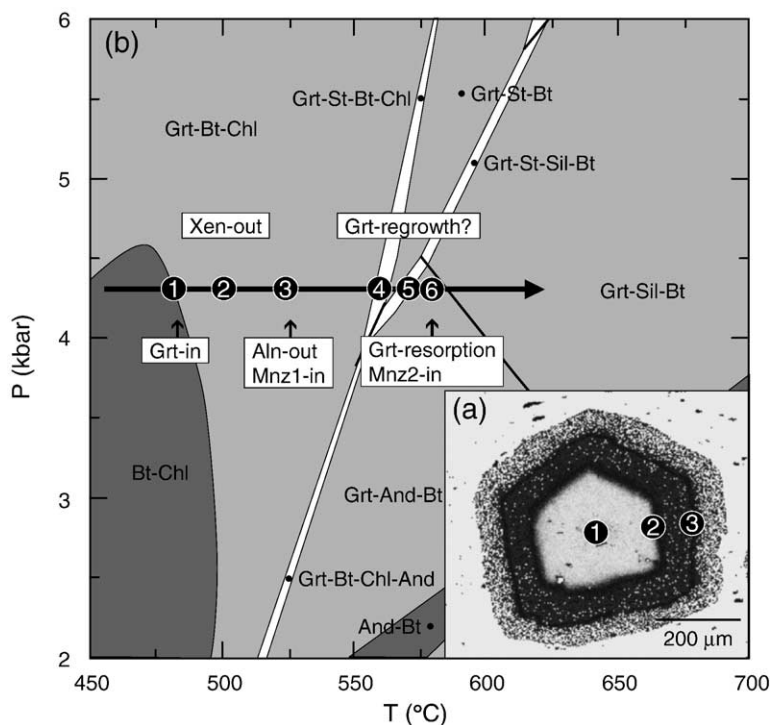
Fig. 12. Summary of parageneses of xenotime, monazite, and allanite in Black Hills along the isobaric heating path at 4.3 kbar. Y maps of (a) B40 and (b) the P–T mineral assemblage diagram of B40 were used to infer the paragenesis.

indicated by the high-Y core in the garnet where inclusions of xenotime were found. The YAG-xenotime thermometer (Pyle and Spear, 2000) applied to the high-Y core gives a temperature of 462 °C, close to the ~480 °C inception of garnet stability in Fig. 12 and peak temperatures (469–500 °C) estimated by Helms and Labotka (1991) in the garnet zone using the garnet–biotite Fe–Mg exchange thermometer. Xenotime leaves the pelite B40 approximately at point 2, resulting in a dramatic decrease in the Y content of garnet. At the time of initial garnet growth, monazite was probably not present because (1) there is no high-Y core in monazite as there is in garnet and (2) the estimated temperature (173 ± 21 °C) using the monazite–xenotime solvus thermometer (Pyle et al., 2001) is unreasonably low. If monazite grew together with garnet in the absence of xenotime, Y zoning in monazite would be expected to follow that of garnet because the growth of garnet fractionates Y from the matrix. The absence of such continuously decreasing Y zoning in monazite suggests that the monazite 1 grew at the expense of allanite at time represented by the formation of Y annuli in garnet. The location and thickness of the Y annuli in B40 suggest that allanite broke down in a narrow range of time relative to garnet growth before the onset of staurolite growth. This allanite–monazite transition is arbitrarily placed in the garnet zone at point 3.

Garnet continued to grow in the garnet zone as indicated by continued crystallization outboard of the Y annuli. Growth of monazite 1, however, was probably slowed down dramatically after the breakdown of allanite because of the exhaustion of LREE in the reservoir. Although garnet is predicted to undergo resorption at point 4 at the onset of the staurolite-forming reaction, the observed degree of garnet resorption is negligible in the sub-aluminous pelites. Garnet is predicted to grow again at point 5, associated with the andalusite-forming reaction. However, the growth of garnet at the andalusite isograd is not evident in garnet from the sub-aluminous pelites. In the sillimanite zone, monazite 2 grows probably at the expense of garnet and monazite inclusions released by garnet porphyroblasts, producing the thin Y-enriched rims (Fig. 9g). Monazite inclusions released by garnet resorption was suggested as a source of additional LREE (McFarlane et al., 2005). The source of U in the monazite 2, however, is problematic because there is no major U source other than zircon in the pelites. Zircon, however, is generally thought to remain as an inert phase below the migmatite zone (Vavra et al., 1999; Hermann and Rubatto, 2003).

5.3. Implications of monazite ages

The paragenesis of monazite in the Black Hills, combined with other studies such as Wing et al. (2003) and Tomkins and Pattison (2005), suggests that the discontinuous breakdown of allanite triggers a major period of monazite growth in the garnet zone shortly after the breakdown of xenotime. The monazite ages in the garnet and staurolite zones, therefore, represent the ages of the monazite-forming reaction at the expense of allanite, rather than the later resorption of garnet at the staurolite isograd. The ages from the monazite 2 represent monazite growth associated with the garnet resorption at the sillimanite zone. With the current precision of electron microprobe dating, it is difficult to identify any differences between the two monazite-forming reactions in the Black Hills, although this would be an avenue worth exploring in regional terrains in which heating rates are slower.

Acknowledgements

References

Andrehs, G., Heinrich, W., 1998. Experimental determination of REE distributions between monazite and xenotime: potential for temperature-calibrated geochronology. Chemical Geology 149, 83–96.

Bea, F., 1996. Residence of REE, Y, Th and U in granites and crustal protoliths: implications for the chemistry of crustal melts. Journal of Petrology 37, 521–552.

Bea, F., Montero, P., 1999. Behavior of accessory phases and redistribution of Zr, REE, Y, Th, and U during metamorphism and partial melting of metapelites in the lower crust: an example from the Kinzigite Formation of Ivrea–Verbano NW Italy. Geochimica et Cosmochimica Acta 63, 1133–1153.

Bea, F., Pereira, M.D., Stroh, A., 1994. Mineral/leucosome trace-element partitioning in a peraluminous migmatite (a laser ablation-ICP-MS study). Chemical Geology 117, 291–312.

Carlson, W., 2002. Scales of disequilibrium and rates of equilibration during metamorphism. American Mineralogist 87, 185–204.

Cesare, B., Marchesi, C., Hermann, J., Gomez-Pugnaire, M.T., 2003. Primary melt inclusions in andalusite from anatectic graphitic metapelites: implications for the position of the Al_2SiO_5 triple point. Geology 31, 573–576.

Chernoff, C.B., Carlson, W.D., 1997. Disequilibrium for Ca during growth of pelitic garnet. Journal of Metamorphic Geology 15, 421–438.

Chernoff, C.B., Carlson, W.D., 1999. Trace element zoning as a record of chemical disequilibrium during garnet growth. Geology 27, 555–558.

Clarke, D.B., et al., 2005. Occurrence and origin of andalusite in peraluminous felsic igneous rocks. Journal of Petrology 46, 441–472.

Connolly, J.A.D., 1990. Calculation of multivariable phase diagrams: an algorithm based on generalized thermodynamics. American Journal of Science 290, 666–718.

Dahl, P.S., Frei, R., 1998. Step-leach Pb–Pb dating of inclusion-bearing garnet and staurolite, with implications for early Proterozoic tectonism in the Black Hills collisional orogen South Dakota, United States. Geology 26, 111–114.

Dahl, P.S., Hamilton, M.A., Jercinovic, M.J., Terry, M.P., Williams, M.L., Frei, R., 2005. Comparative isotopic and chemical geochronometry of monazite, with implications for U–Th–Pb dating by electron microprobe: an example from metamorphic rocks of the eastern Wyoming (U.S.A.). American Mineralogist 90, 619–638.

Deer, W.A., Howie, R.A., Zussman, J., 1992. An introduction to the rock forming minerals, 2nd edition Wiley and Sons, Inc, New York. 696 pages.

DeWitt, E., Redden, J.A., Wilson, A.B., Buscher, D., 1986. Mineral resource potential and geology of the Back Hills National Forest, South Dakota and Wyoming. U.S. Geological Survey Bulletin, vol. 1580. 135 pp.

DeWitt, E., Redden, J.A., Buscher, D., Wilson, A.B., 1989. Geologic map of the Black Hills area, South Dakota and Wyoming: U.S. Geological Survey Miscellaneous Investigations Series Map I-1910, scale 1:250,000.

Duke, E.F., Redden, J.A., Papike, J.J., 1988. Calamity Peak layered granite–pegmatite complex, Black Hills, South Dakota: Part I. Structure and emplacement. Geological Society of America Bulletin 100, 825–840.

Ferry, J.M., 2000. Patterns of mineral occurrence in metamorphic rocks. American Mineralogist 85, 1573–1588.

Finger, F., Broska, I., Roberts, M.P., Schermaier, A., 1998. Replacement of primary monazite by apatite–allanite–epidote coronas in an amphibolite facies granite gneiss from the eastern Alps. American Mineralogist 83, 248–258.

Fraser, G.L., Pattison, D.R.M., Heaman, L.M., 2004. Age of the Ballachulish and Glencoe Igneous Complexes (Scottish Highlands), and paragenesis of zircon, monazite and baddeleyite in the Ballachulish Aureole. Journal of the Geological Society of London 161, 447–462.

Gratz, R., Heinrich, W., 1997. Monazite–xenotime thermobarometry; experimental calibration of the miscibility gap in the system CePO4–YPO4. American Mineralogist 82, 772–780.

Gratz, R., Heinrich, W., 1998. Monazite–xenotime thermometry: III. Experimental calibration of the partitioning of gadolinium between monazite and xenotime. European Journal of Mineralogy 10, 579–588.

Heinrich, W., Andrehs, G., Franz, G., 1997. Monazite–xenotime miscibility gap thermometry. I. An empirical calibration. Journal of Metamorphic Geology 15, 3–16.

Helms, T.S., Labotka, T.C., 1991. Petrogenesis of Early Proterozoic pelitic schists of the southern Black Hills, South Dakota: constraints on regional low-pressure metamorphism. Geological Society of America Bulletin 103, 1324–1334.

Hermann, J., Rubatto, D., 2003. Relating zircon and monazite domains to garnet growth zones: age and duration of granulite facies metamorphism in the Val Malenco lower crust. Journal of Metamorphic Geology 21, 833–853.

Hickmott, D.D., Spear, F.S., 1992. Major- and trace-element zoning in garnets from calcareous pelites in the NW Shelburne Falls quadrangle, Massachusetts: garnet growth histories in retrograded rocks. Journal of Petrology 33, 965–1005.

Hickmott, D.D., Shimizu, N., Spear, F.S., Selverstone, J., 1987. Trace-element zoning in a metamorphic garnet. Geology 15, 573–576.

Hirsch, D.M., Prior, D.J., Carlson, W.D., 2003. An overgrowth model to explain multiple, dispersed high-Mn regions in the cores of garnet porphyroblasts. American Mineralogist 88, 131–141.

Holland, T.J.B., Powell, R., 1990. An enlarged and updated internally consistent thermodynamic dataset with uncertainties and correlations: the system K_2O-Na_2O-CaO-MgO-MnO-FeO-Fe_2O_3-Al_2O_3-TiO_2-SiO_2-C-H_2O-O_2. Journal of Metamorphic Geology 8, 89–124.

Holland, T.J.B., Powell, R., 1998. An internally consistent thermodynamic data set for phases of petrological interest. Journal of Metamorphic Geology 16, 309–343.

Kohn, M.J., Malloy, M.A., 2004. Formation of monazite via prograde metamorphic reactions among common silicates: implications for age determinations. Geochimica et Cosmochimica Acta 68, 101–113.

Kretz, R., 1983. Symbols of rock-forming minerals. American Mineralogist 68, 277–279.

Mahar, E.M., Baker, J.M., Powell, R., Holland, T.J.B., Howell, N., 1997. The effect of Mn on mineral stability in metapelites. Journal of Metamorphic Geology 15, 223–238.

McFarlane, C.R.M., Connelly, J.N., Carlson, W.D., 2005. Monazite and xenotime petrogenesis in the contact aureole of the Makhavinekh Lake Pluton, northern Labrador. Contributions to Mineralogy and Petrology 148, 524–541.

Menard, T., Spear, F.S., 1993. Metamorphism of calcic pelitic schists, Strafford Dome, Vermont: compositional zoning and reaction history. Journal of Petrology 34, 977–1005.

Nabelek, P.I., Labotka, T.C., Helms, T.S., Wilke, M., 2005. Fluid-mediated mineral consumption and growth in polymetamorphosed metapelites of the Black Hills, South Dakota. 15th Goldschmidt Conference (Moscow, Idaho), Abstracts Volume, p. A407.

Newton, R.C., Charlu, T.V., Kleppa, O.J., 1980. Thermochemistry of the high structural state plagioclases. Geochimica et Cosmochimica Acta 44, 933–941.

Pattison, D.R.M., 1992. Stability of andalusite and sillimanite and the Al_2SiO_5 triple point: constraints from the Ballachulish aureole, Scotland. Journal of Geology 100, 423–446.

Pattison, D.R.M., Tracy, R.J., 1991. Phase equilibria and thermobarometry of metapelites. In: Kerrick, D.M. (Ed.), Contact Metamorphism, Reviews in Mineralogy, vol. 26. Mineralogical Society of America, pp. 105–206.

Powell, R., Holland, T., 1999. Relating formulations of the thermodynamics of mineral solid solutions: activity modeling of pyroxenes, amphiboles and micas. American Mineralogist 84, 1–14.

Pyle, J.M., Spear, F.S., 1999. Yttrium zoning in garnet: coupling of major and accessory phases during metamorphic reactions. Geological Materials Research 1, 1–49.

Pyle, J.M., Spear, F.S., 2000. An empirical garnet (YAG)–xenotime thermometer. Contributions to Mineralogy and Petrology 138, 51–58.

Pyle, J.M., Spear, F.S., 2003. Four generations of accessory-phase growth in low-pressure migmatites from SW New Hampshire. American Mineralogist 88, 338–351.

Pyle, J.M., Spear, F.S., Rudnick, R.L., McDonough, W.F., 2001. Monazite–xenotime–garnet equilibrium in metapelites and a new monazite–garnet thermometer. Journal of Petrology 42, 2083–2107.

Rasband, W., 1998. Scion Image. http://www.scioncorp.com.

Redden, J.A., Norton, J.J., McLaughlin, R.J., 1982. Geology of the Harney Peak granite, Black Hills, South Dakota. U.S. Geological Survey Open-File Report 82-481. 18 pp.

Redden, J.A., Peterman, Z.E., Zartman, R.E., DeWitt, E., 1990. U–Th–Pb zircon and monazite ages and preliminary interpretation of the tectonic development of Precambrian rocks in the Black Hill. In: Lewry, J.F., Stauffer, M.R. (Eds.), The Early Proterozoic Trans-Hudson Orogen, Geological Association of Canada Special Report, vol. 37, pp. 229–251.

Schwandt, C.S., Papike, J.J., Shearer, C.K., 1996. Trace element zoning in pelitic garnet of the Black Hills, South Dakota. American Mineralogist 81, 1195–1207.

Shaw, D.M., 1956. Geochemistry of pelitic rocks: Part III. Major elements and general geochemistry. Bulletin of the Geological Society of America 67, 919–934.

Shearer, C.K., Papike, J.J., Jolliff, B.L., 1992. Mineralogical and chemical evolution of the Harney Peak rare element granite–pegmatite system, Back Hills, South Dakota: petrgenetic links between granites and pegmatites. Canadian Mineralogist 30, 785–810.

Smith, H.A., Barreiro, B., 1990. Monazite U–Pb dating of staurolite grade metamorphism in pelitic schists. Contributions to Mineralogy and Petrology 105, 602–615.

Spear, F.S., Cheney, J.T., 1989. A petrogenetic grid for pelitic schists in the system SiO_2–Al_2O_3–FeO–MgO–K_2O–H_2O. Contributions to Mineralogy and Petrology 101, 149–164.

Spear, F.S., Kohn, M.J., Florence, F., Menard, T., 1990. A model for garnet and plagioclase growth in pelitic schists: implications for thermbarometry and P–T path determinations. Journal of Metamorphic Geology 8, 683–696.

Spear, F.S., Kohn, M.J., Cheney, J.T., 1999. P–T paths from anatectic pelites. Contributions to Mineralogy and Petrology 134, 17–32.

Symmes, G.H., Ferry, J.M., 1992. The effect of whole-rock MnO content on the stability of garnet in pelitic schists during metamorphism. Journal of Metamorphic Geology 10, 221–237.

Terry, M.P., Friberg, L.V.M., 1990. Pressure–temperature–time path related to the thermotectonic evolution of an Early Proterozoic metamorphic terrane, Black Hills, South Dakota. Geology 18, 786–789.

Thompson, J.B. Jr., 1957. The graphical analysis of mineral assemblages in pelitic schists. American Mineralogist 42, 842–858.

Tinkham, D.K., Zuluaga, C.A., Stowell, H.H., 2001. Metapelite phase equilibria modeling in MnNCKFMASH: the effect of variable Al_2O_3 and MgO/(MgO+FeO) on mineral stability. Geological Materials Research 3, 1–41.

Tomkins, H.S., Pattison, D.R.M., 2005. Monazite petrogenesis in the Nelson contact aureole, southern British Columbia. 15th Goldschmidt Conference (Moscow Idaho), Abstracts Volume, p. A400.

Vance, D., Mahar, E., 1998. Pressure–temperature paths from P–T pseudosections and zoned garnets: potential, pitfalls and examples from the Zanskar Himalaya, NW India. Contributions to Mineralogy and Petrology 132, 225–245.

Vavra, G., Schmidt, R., Gebauer, D., 1999. Internal morphology, habit and U–Th–Pb microanalysis of amphibolite-to-granulite facies zircons: geochronology of the Ivera Zone (Southern Alps). Contributions to Mineralogy and Petrology 134, 380–404.

Wing, B.A., Ferry, J.M., Harrison, T.M., 2003. Prograde destruction and formation of monazite and allanite during contact and regional metamorphism of pelites: petrology and geochronology. Contributions to Mineralogy and Petrology 145, 228–250.

Yang, P., Rivers, T., 2000. Trace element partitioning between coexisting biotite and muscovite from metamorphic rocks, western Labrador: structural, compositional and thermal controls. Geochimica et Cosmochimica Acta 64, 1451–1472.

Yang, P., Rivers, T., 2001. Chromium and manganese zoning in pelitic garnet and kyanite: spiral, overprint, and oscillatory (?) zoning patterns and the role of growth rate. Journal of Metamorphic Geology 19, 455–474.

Yang, P., Rivers, T., 2002. The origin of Mn and Y annuli in garnet and the thermal dependence of P in garnet and Y in apatite in calc-pelite and pelite. Gagnon terrane, western Labrador. Geological Materials Research 4, 1–35.

Yang, P., Rivers, T., Jackson, S., 1999. Crystal–chemical and thermal controls on trace-element partitioning between coexisting garnet and biotite in metamorphic rocks from western Labrador. Canadian Mineralogist 37, 443–468.